

Airfoil Lift Calculation Using Wind Tunnel Wall Pressures

Proc. IMechE Part G: J. Aerospace
Engineering
XX(X):1–11
©The Author(s) 2020
Reprints and permission:
sagepub.co.uk/journalsPermissions.nav
DOI: 10.1177/ToBeAssigned
www.sagepub.com/

SAGE

Sreevishnu Oruganti¹ and Shreyas Narsipur²

Abstract

An experimental method to calculate lift using static pressure ports on the wind tunnel walls and its associated limits has been explored in this paper. While the wall-pressure measurement (WPM) technique for lift calculation has been implemented by other researchers, there is a lack of literature on the sensitivity of the WPM method to test section size, airfoil chord, and model thickness. Chord sensitivity studies showed that the airfoil chord plays an important role in the accuracy of the measurements and needs to be appropriately sized for a given test section dimensions for optimum performance of the WPM method. A chord sensitivity parameter (CSP) was formulated and a lower limit ($= 0.025$) was established to relate the ideal chord-length to wind tunnel test-section dimensions to ensure best lift measuring capabilities. Finally, a combination of symmetric and cambered airfoils with thicknesses varying from 6% – 21% were tested and successfully validated against reference data for a freestream chord Reynolds number range of 100,000 to 550,000. The WPM method was found to be sensitive to varying surface flow conditions and airfoil thickness and has been shown to be a viable replacement to traditional lift measurement techniques using load balances or surface pressure ports.

Keywords

Wind Tunnel Testing, Airfoil Lift, Wall Pressure Measurement, Chord Sensitivity Parameter, Validation

1 Introduction

In aerodynamics, the calculation of lift is important as it greatly influences the design of aerial vehicles. Conventionally, lift on an airfoil is measured in wind tunnels using either load balances or airfoil surface pressure ports. While the load balance method is popular, the method requires constant calibration to ensure the accuracy of the force results being measured^{1,2}. On the other hand, while surface pressure measurements offer the capability of measuring the lift while giving a better insight into the surface aerodynamics, manufacturing and maintaining the models with the surface pressure ports can be very time consuming and expensive. Additionally, the pressure ports can cause surface roughness that in turn could lead to premature flow transition and affect laminar bubble formation³ in steady flows and additionally affect leading-edge vortex dynamics in unsteady flow conditions, ultimately affecting the lift behavior.

The Wall Pressure Measurement (WPM) method to measure airfoil lift has been successfully implemented in the Stuttgart University⁴, NASA Langley⁵, and Oldenburg University wind tunnels^{6–8}. When air flows around an airfoil, gradients in the flow velocity are created around the airfoil, with a high pressure region on the lower surface of the airfoil and a low pressure region on the upper surface, causing a net upward force, called lift. Perturbations in the flow velocity due to the presence of an airfoil in a wind tunnel test section will affect flow at the test section walls. In the WPM method, static pressures are recorded at the walls of the wind tunnel in order to capture the projected flow velocities due to the presence of the airfoil. The airfoil lift can then be measured

by integrating the static pressure distributions at the walls and applying the relevant correction factors⁴.

As the setup used for the WPM method is on the walls of the wind tunnel and not directly on the airfoil, as in the Surface Pressure Measurement (SPM) method, or attached to the airfoil, as in the Load Cell Measurement (LCM) method, the WPM method provides a very non-intrusive way of obtaining the airfoil lift without affecting the flow near the airfoil. Literature shows that the WPM method has also been effectively used to study wind tunnel blockage effects and corrections for velocity, pressure, lift and drag for vertical axis wind turbines (VAWTs), rotorcrafts, and other 2-dimensional and 3-dimensional bodies^{9–16}. The WPM method offers the additional possibility of capturing the effective shape of the airfoil as seen by the flow, as the pressure ports on the walls capture the separated or stagnant air around the airfoil along with the pressures caused by the airfoil. This can then be used to identify laminar bubbles, leading-edge separation bubbles, etc., which can be very useful for testing unsteady characteristics of airfoils^{6,7}. Furthermore, these wall pressures can be used in theoretical models or machine learning models to compute the airfoil

¹North Carolina State University, USA

²North Carolina State University, USA

Corresponding author:

Shreyas Narsipur, North Carolina State University, Raleigh, NC 27695, USA.

Email: shreya@ncsu.edu

surface pressures, airfoil forces and moments, and even the full flow field in the test-section.

In spite of the WPM method's popularity and possibilities, little to no literature exists on the sensitivity and predictive capabilities of the WPM method to the airfoil geometry, test section dimensions, and flow conditions. Parametric studies exploring the above conditions will help inform researchers of the testing limits and capabilities of the WPM system. In the current research, a WPM test bench is retrofitted and validated in the NCSU low-speed wind tunnel. Initial efforts were focused on conducting a chord sensitivity study to determine the optimal airfoil chord to test section dimensions ratio that will allow for the WPM system to be accurate and feasible to implement. A consistent parameter and its associated limits are explored that can relate test-section dimensions to airfoil section sizing for optimal performance of the WPM system. Subsequent efforts were focused on validating the C_l measured using the WPM test bench against Surface Pressure Measurement (SPM) and Load Cell Measurement (LCM) data for eight airfoil sections with varying thickness and camber. Additionally, the prediction accuracy of the WPM method in the presence of auxiliary surfaces on the airfoil such as tripwires, vortex generators, etc., was tested.

The following section (Section 2) discusses the theory behind the WPM technique and its implementation at the NCSU wind tunnel facility. Sections 3 and 4 present the results from the chord sensitivity and the validation studies, respectively. The final section (Section 5) presents the conclusions drawn and suggests possible future directions for the current research.

2 Methodology and Experimental Setup

In this section, the methodology behind the WPM method in calculating static airfoil lift is described. Details with regard to the wind tunnel, the theory and equations used and the implemented WPM setup are presented in subsections 2.1, 2.2 and 2.3 respectively.

2.1 Wind Tunnel Specifications

Experimental investigations were conducted in the North Carolina State University's closed-circuit, subsonic wind tunnel facility which has a 3:1 contraction ratio and a test section measuring $46 \times 45 \times 32$ inches (length \times width \times height). The wind tunnel is capable of reaching freestream velocities of up to 90 mph via a 3-blade, varying pitch propeller driven by a 250 horsepower electric motor. The settling chamber is equipped with a honeycomb screen and two anti-turbulence screens to ensure good flow quality. The turbulence intensity, based on turbulence sphere and hot-wire anemometry tests, has been measured to be 0.3%. Pressure measurements were made using three, 16-port Scanivalve DSA3217 systems with a $\pm 0.05\%$ accuracy¹⁷. The converging and test sections of the wind tunnel is shown on Fig. 1.



Figure 1. The NC State University subsonic wind tunnel.

2.2 Theory and Equations

The method for deducing the airfoil lift using wall pressure ports is similar to that using surface pressure ports, with the added advantage of inexpensive airfoil models that can be rapidly manufactured. The static pressure gradient caused by the airfoil's upper and lower surfaces are measured and integrated to calculate the non-dimensionalized net upward force, or the lift coefficient, of the airfoil. However, as the circulation of the airfoil theoretically extends to infinity but the integration is performed only over the restricted length across which the pressure ports are distributed along the wind tunnel walls, correction factors as described by Althaus⁴ are applied to deduce the final airfoil lift coefficient. These correction factors assume that the airfoil is mounted such that centers of the airfoil and the wind tunnel test section are aligned.

On obtaining the static pressures from the upper (P_{upper}) and lower (P_{lower}) wind tunnel walls, parallel to the airfoil chord, the uncorrected coefficient of lift of the airfoil can be calculated as:

$$C_{l,wall} = \frac{1}{q_{\infty}} \int_m^n (P_{upper} - P_{lower}) \cdot \frac{dx}{l} \quad (1)$$

where m and n are the horizontal distances from the airfoil center to the left- and right-most wall pressure ports, respectively, and l is the distance between the first and last wall pressure ports, as illustrated in Fig. 2.

To translate the lift coefficient based on the wall pressure measurements ($C_{l,wall}$) to the actual airfoil lift coefficient ($C_{l,corr}$), two correction factors, commonly referred to as the Althaus factors⁴, need to be applied. These factors, determined by decomposing the airfoil's pressure distribution at the wall into a basic, constant distribution and a distribution due to the effect of the airfoil's angle of attack, are calculated using the equations,

$$\eta_a = \int_0^c \frac{2}{\pi} \cdot \sqrt{\frac{1 - \frac{x}{c}}{\frac{x}{c}}} \cdot \eta_x \cdot \frac{dx}{c} \quad (2)$$

$$\eta_b = \int_0^c 1 \cdot \eta_x \cdot \frac{dx}{c} \quad (3)$$

where η_x is the correction factor at a given location on the wall and is dependent on the horizontal distance between the

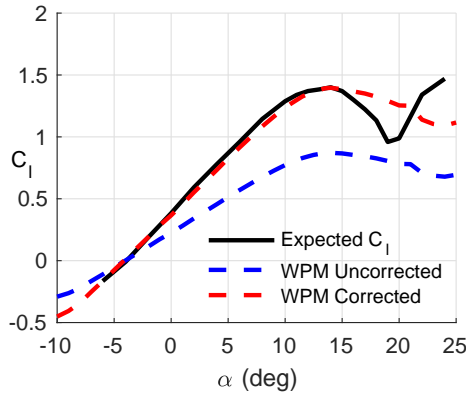


Figure 5. Uncorrected and corrected WPM method results comparison with SPM results for $Re = 250,000$.

(LRN) cambered airfoil was taken as the baseline geometry as a 12-inch chord version of the airfoil model with 44 surface pressure ports was available at the NCSU wind tunnel facility, thereby providing a commensurable way to compare the WPM predictions with SPM results. The symmetric, 12% thick NACA 0012 airfoil was also considered for the initial validation and chord sensitivity study as a plethora of LCM datasets were available^{19–24} at the required Reynolds number range. Four versions of each of the two airfoils with 6-, 8-, 10-, and 12-inch chord lengths were 3D printed using ABS plastic with two support rods at the quarter- and three-quarter-chord locations to prevent bending or warping. The Althaus correction factors and the scaling ratios for each of the chord length's is listed in Table 1.

Table 1. Correction Factors and Scaling Ratios for Different Chord Lengths

Chord (in.)	Althaus-Correction Factor (η_a)	Scaling Ratio (sr), %
6	0.6537	15
8	0.6525	20
10	0.6501	25
12	0.6491	30

Figure 5 shows representative uncorrected and corrected lift results ($C_{l,wall}$ and C_l , respectively) from the WPM method for the 12-inch chord airfoil compared to the lift obtained from SPM data for the LRN airfoil at a Reynolds number of 250,000 to illustrate the steps in the WPM method to obtain airfoil C_l . Both the uncorrected and the corrected results follow similar trends, stall at the same angle of attack and predict zero-lift angle accurately. Additionally, corrected C_l data from the WPM method is in good agreement with SPM results up to and slightly beyond stall (up to $\alpha = 16$ degrees) but deviates at higher angles of attack.

Figure 6 plots the (a) C_l versus α results from the WPM for different airfoil chord lengths compared with SPM measurements and (b) absolute errors in $C_{l,max}$ and α_{stall} along with the overall sum of square errors (SSE) against airfoil chord to investigate the WPM method's sensitivity to chord variation. The SSE between the WPM and expected results is determined using the equation,

$$SSE = \sum_1^N \left(\frac{\sum_1^N (C_{l,exp} - C_l)}{N} - (C_{l,exp} - C_l) \right)^2 \quad (8)$$

where $C_{l,exp}$ is the expected lift coefficient value obtained from reference data, C_l is the lift coefficient from the WPM method and N is the number of data points considered for taking the SSE. Observations from Fig. 6(a) show that, independent of chord length, the WPM results exhibit slight to no variance in zero-lift angle of attack and the linear lift curve slope at the attached flow conditions. As α_{stall} is approached, the sensitivity of the WPM method is evident, with the 6-inch chord airfoil severely underpredicting α_{stall} .

This can be further verified from observations of Fig. 6(b) where, while the error in $C_{l,max}$ predictions are $\leq 5\%$ with a slight decrease for $c > 8$ -inches, the error in α_{stall} is $\approx 15\%$ for the 6-inch followed by a sharp drop for the larger chord lengths and close to zero error for $c \geq 10$ -inches. Post-stall predictions for all airfoil chords aberrate from expected results with the magnitude of deviation captured by the SSE in Fig. 6(b). Overall SSE is the least for the 8-inch chord and maximum for the 10-inch chord with the SSE predominantly depending on the post-stall lift behavior. The 6-inch airfoil accurately predicts the C_l for $17 \leq \alpha \leq 20$ degrees while the other airfoils overpredict from right after stall to $\alpha = 22$ degrees. For $\alpha > 22$ degrees, all airfoils underpredict C_l in comparison to SPM results.

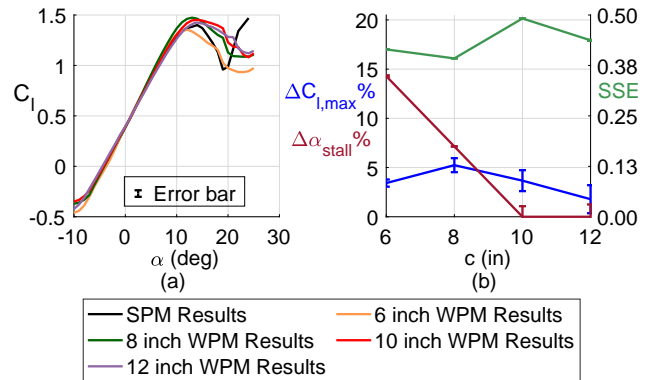


Figure 6. LRN chord sensitivity study at $Re = 250,000$. (a) C_l vs α for 4 different chord lengths, (b) the corresponding errors in $C_{l,max}$, α_{stall} and SSE.

On performing a similar analysis at a Reynolds number of 400,000 for the LRN airfoil (Fig. 7), we observe that while C_l prediction trends for $c \geq 8$ -inches are similar to the $Re = 250,000$ case, the predictions for the 6-inch airfoil case improve significantly. All airfoils accurately predict C_l up to stall ($\alpha = 14$ degrees), overpredict for $14 < \alpha < 20$ degrees, and underpredict for $\alpha \geq 20$ degrees. $C_{l,max}$ errors are consistently below 5% for all chord lengths while α_{stall} errors are above 10% for $c = 6$ -inches followed by a reduction to $\approx 0\%$ at $c = 10$ -inches and a slight increase for the higher chord length. SSE magnitudes are lower at $Re = 400,000$ with maximum (at $c = 8$ -inches) and minimum (at $c = 12$ -inches) values of 0.340 and 0.145, respectively.

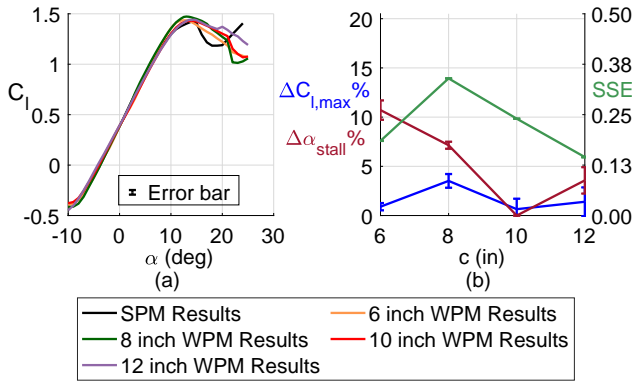


Figure 7. LRN chord sensitivity study at $Re = 400,000$. (a) C_l vs α for 4 different chord lengths, (b) the corresponding errors in $C_{l,max}$, α_{stall} and SSE.

The improvement observed in C_l predictions for the 6-inch airfoil is interesting and can be attributed to the low scaling ratio ($sr = 15$) and high Reynolds number. At angles of attack close to stall, the airfoil experiences a loss in surface pressure due to flow separation. At lower Reynolds numbers, the magnitude of the airfoil surface pressure at these higher angles of attack are lower as compared to that at higher- Re cases, due to which the resulting flow perturbation magnitudes at the wind tunnel walls are lower. Therefore, at higher Reynolds numbers, the wall pressure ports better capture the projected airfoil pressure distributions and predict the associated lift characteristics more accurately. This will not be an issue for the larger chord length airfoils as the scaling is large enough to overcome the Reynolds number dependency of the WPM method.

C_l versus α and associated errors between the WPM predictions and LCM data for the NACA 0012 airfoil at $Re = 330,000$ for different chord lengths are plotted in Fig. 8. While C_l trends are seen to be almost independent of airfoil chord (Fig. 8(a)), the lift is accurately predicted until $\alpha = 9$ degrees after which the WPM results slightly deviate from expected results. Additionally, the WPM results show a sharper stall behavior as compared to the LCM data. As airfoil stall is sensitive to wind tunnel conditions, the variation in stall behavior can be attributed to the difference in testing facilities. Figure 8(b) shows that the SSE magnitudes are comparatively lower to those observed for the LRN airfoil cases as post-stall predictions are better for the NACA 0012 airfoil. However, $C_{l,max}$ is overpredicted by at least 12% ($c = 10$ -inches) and α_{stall} is $\approx 1\%$ for $c = 8$ -inches and higher than 8% for all other chord lengths.

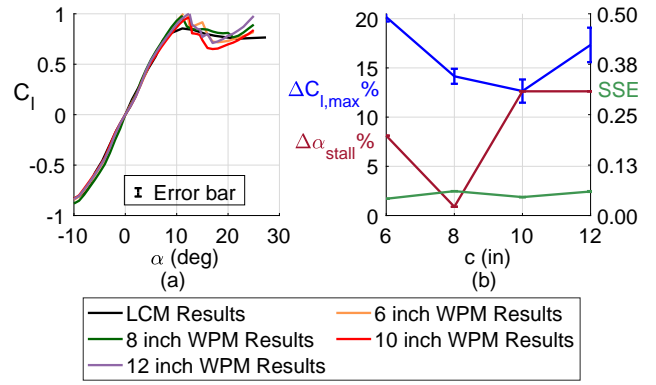


Figure 8. NACA 0012 chord sensitivity study at $Re = 330,000$ ¹⁹. (a) C_l vs α for 4 different chord lengths, (b) the corresponding errors in $C_{l,max}$, α_{stall} and SSE.

Based on the above results, it can be deduced that, while SSE data informs us of the overall match between the predicted and expected results, it alone is not sufficient to draw conclusions on which sr combination is optimum for testing purposes, mainly evidenced by the results for the 6-inch airfoil model which shows low SSE magnitudes but significantly under/overpredicts $C_{l,max}$ and α_{stall} . Furthermore, though predictions for airfoils with lower sr values improve as the Reynolds number increases, it is not recommended to test with similarly sized airfoil models as, in addition to their unsuitability for low Reynolds number experiments, they will require the wind tunnel to operate at higher dynamic pressure settings for a given Reynolds number, which in turn can result in high variations in testing conditions due to temperature build-up in the test section and wind tunnel vibrations. Additionally, LRN results show moderate prediction accuracy for $c = 8$ -inches ($sr = 20$) and high prediction accuracy for $c \geq 10$ -inches ($sr \geq 25$) while NACA 0012 results show the best accuracy for the $c = 8$ inches ($sr = 20$) case. Therefore, for subsequent studies in this work, airfoil test sections with 8-inch chord lengths were manufactured as it provides a good trade-off between prediction accuracy and manufacturing costs (due to low 3D printing material usage).

3.1 Chord Sensitivity Parameter

As one of the aims of the current work was to establish chord-sizing rules to accurately test airfoils using the WPM method, efforts were focused on defining a parameter that can be used to inform researchers on the optimal airfoil chord length for a given wind tunnel test section dimensions. From the above chord sensitivity study, it was seen that for the NCSU wind tunnel, the WPM method results were most accurate for sr values above 20. However, the sr value for the WPM setups at the NASA Langley⁵ and Oldenburg University wind tunnels⁶⁻⁸ were found to be 15.4% and 10%, respectively. Further inspection of the WPM setups in the three wind tunnels revealed that, in addition to different test section lengths, the width of the wind tunnel test sections in all three cases were different. This indicated a possible link between the wind tunnel width and accuracy of the WPM predictions. Therefore, a Chord Sensitivity Parameter (CSP) given by the equation,

$$CSP = \frac{c^2}{w * l} \quad (9)$$

was defined. Based on Eqn. 9, the lower limit of CSP was evaluated to be 0.0389 for the current wind tunnel setup. While the limit in CSP agreed with the NASA wind tunnel setup ($CSP = 0.041$), it did not do so with that of the Oldenburg wind tunnel ($CSP = 0.025$). It is recognized that, due to the restriction for the NCSU wind tunnel, more combinations for c , w and l could not be considered. Given this being the case, we define the lower limit of the CSP to be equal to that corresponding to the Oldenburg wind tunnel and conclude that for the WPM setup, the airfoil chord should be modeled such that the $CSP \geq 0.025$. While no upper limit can be established with current knowledge, there will exist one as larger airfoil-chords will have the tendency to affect wall pressures beyond the tunnel length and failing to capture them will result in incorrect C_l predictions.

4 WPM Setup Validation

In order to thoroughly validate the WPM setup, a combination of eight symmetric and cambered airfoils with thicknesses ranging from 6% to 12% were tested. Additionally, three airfoils were also tested in tripped-flow conditions. Subsection 4.1 provides details of the airfoil geometries tested along with the associated freestream conditions. Comparison of the C_l results from the WPM method with SPM and LCM data from the current research and literature are discussed in Section 4.2 to determine the validity of the current WPM setup.

4.1 Airfoils Tested

Based on the chord sensitivity study (Section 3), eight 8-inch chord wing models with different airfoil sections were manufactured with ABS plastic using 3D printing techniques and were reinforced with support rods spanning the length of the model. Table 2 provides details pertaining to the airfoil geometries, test conditions at which measurements were taken, and the reference data against which the WPM results were compared. Note that, for the 8-inch chord sections, the freestream Reynolds number was restricted to 550,000 in order to ensure good flow quality. Pressure data was collected at angles of attack ranging from -10 degrees to 25 degrees in 1 degree intervals for all airfoils.

4.2 Validation Study

The current section presents the lift coefficient results predicted by the WPM test bench and validates them against experimental SPM and LCM data. For all of the validation study results shown in this section, C_l vs α plots are shown for two or more Reynolds numbers for α varying from -10 degrees to 25 degrees. Additionally, the error bars for the lift coefficient at every alternate angle of attack are plotted.

4.2.1 LRN Airfoil ($t/c = 12\%$) Results of the 8-inch WPM model compared to those obtained by integrating the surface pressure measurements of the LRN 12-inch, surface pressure model for Reynolds numbers ranging from 250,000 to 500,000 are presented in Fig. 9. Observations

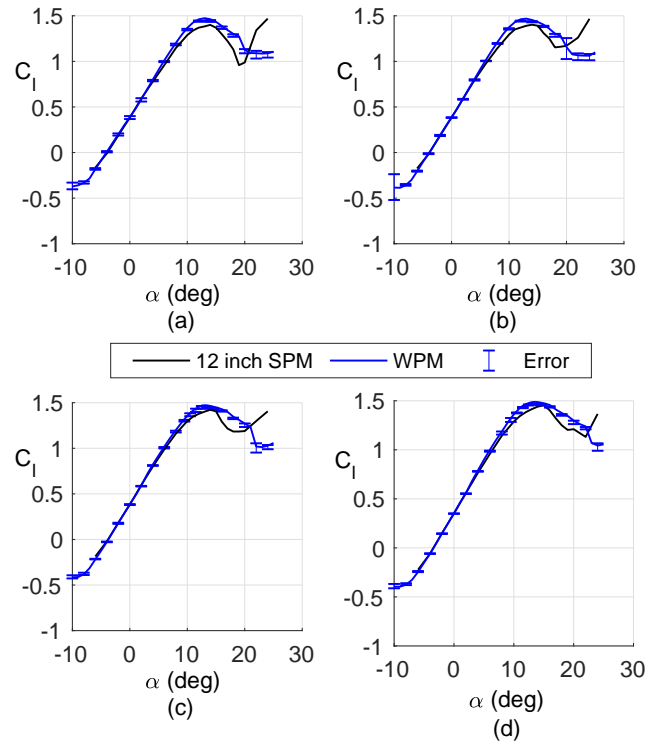


Figure 9. Comparison study of SPM results vs WPM results for LRN airfoil at (a) $Re = 250,000$, (b) $Re = 300,000$, (c) $Re = 400,000$, and (d) $Re = 500,000$ ¹⁷.

show the WPM method results match up very well with the surface pressure results at lower angles of attack (-5 degrees to 10 degrees) at all Reynolds numbers. Small variations are observed for angles of attack greater than 10 degrees with the WPM method slightly overpredicting the maximum C_l at all freestream Reynolds number conditions. However, predictions are seen to improve with increase in Reynolds number. Figure 9 also shows that key airfoil lift characteristics such as zero-lift angle, lift curve slope, and stall angle are accurately predicted for all Reynolds numbers, barring $Re = 500,000$ (Fig. 9(d)), where the WPM method predicts the stall to occur at a slightly lower angle of attack. A possible reason for the divergence could be due to the small vibrations in the model that were observed at the high Reynolds number conditions.

Post-stall C_l predictions deviate from expected results, both in terms of magnitude and trends. SPM results show the C_l dropping after the airfoil stalls, followed by a rapid to gradual increase, depending on the Reynolds number. However, WPM results predict a continuous drop in C_l until $\alpha \approx 22$ degrees after which it flattens out. The reason for this discrepancy will be investigated in future work.

4.2.2 NACA 0012 ($t/c = 12\%$) WPM results were compared with experimental C_l data from LCM methods^{19–22} for the symmetric NACA 0012 for a Reynolds number range of 170,000 to 550,000, in Fig. 10. It is observed that, at lower angles of attack (-5 degrees to 9 degrees), the C_l is accurately measured by the WPM method at all Reynolds numbers. For $Re = 170,000$, stall angle ($\alpha_{stall} = 11$ degrees) is precisely captured while $C_{l,max}$ is overpredicted by 9% (Fig. 10(a)). WPM results at $Re = 330,000$ show that α_{stall} is underpredicted by 1 degrees and $C_{l,max}$ is overpredicted by 14% (Fig. 10(b)). At Reynolds numbers of 500,000 and

Table 2. Airfoils Tested.

Airfoil	Thickness %	Reynolds Number	Reference
LRN	12	250,000 300,000 400,000 500,000	SPM measurements
NACA0012	12	170,000 330,000 500,000 550,000	Jacobs et al. ¹⁹ Critzos et al. ²⁰ Poisson et al. ²¹
SA7024	8	100,000 300,000	Gopalathnam et al. ²⁵
E387	9	200,000 500,000	Selig et al. ²⁶
Clark Y	12	300,000 400,000	Selig ²⁷
Gemini	15	200,000 300,000	Selig et al. ²⁸
NACA0018	18	250,000 500,000	Boutilier et al. ²⁹ Timmer et al. ³⁰
S823	21	300,000 400,000	Selig et al. ^{28,31}

550,000 (Figs. 10(c) and (d)), stall angles are predicted at 14 degrees by the WPM method, which is 2 degrees over LCM predictions. C_l is overpredicted by 7% and 2% for the $Re = 500,000$ and $Re = 550,000$ cases, respectively. Post-stall WPM results show excellent comparison with the reference data at all Reynolds number conditions, with the predictions within the expected error range of the measurements. At angles of attack below -6 degrees, the WPM method underpredicts the C_l by a small magnitude for the Reynolds number 500,000 and 550,000 cases. Overall, WPM C_l predictions are in good agreement with reference LCM experimental data for the symmetric NACA 0012 airfoil at

all Reynolds number for which the validation studies were conducted.

4.2.3 SA7024 ($t/c = 6\%$) The SA7024 is a 6% thick airfoil designed for low Reynolds number flows. Reference lift data for the SA7024 was collected in the UIUC low-speed wind tunnel and the lift measurements were made using a load balance²⁵. Figure 11 shows that, for all positive angles of attack, the WPM results compare well with the load balance results at both Reynolds numbers. WPM underpredicts C_l for $\alpha < -5$ degrees and seems to indicate an earlier stall during negative angle of attack operation. Deviation in C_l , post-stall, is seen to be higher at

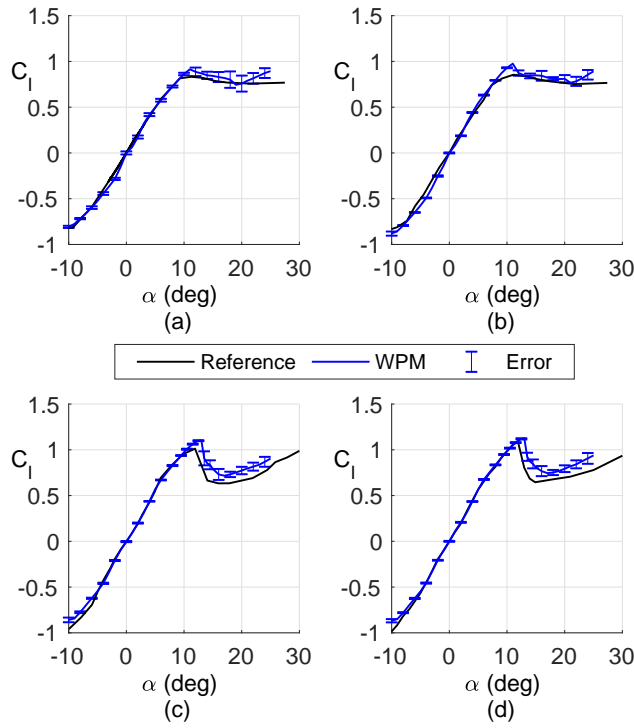


Figure 10. Comparison study of LCM results vs WPM results for NACA 0012 airfoil at (a) $Re = 170,000$ ¹⁹, (b) $Re = 330,000$ ¹⁹, (c) $Re = 500,000$ ²⁰ and (d) $Re = 550,000$ ²¹.

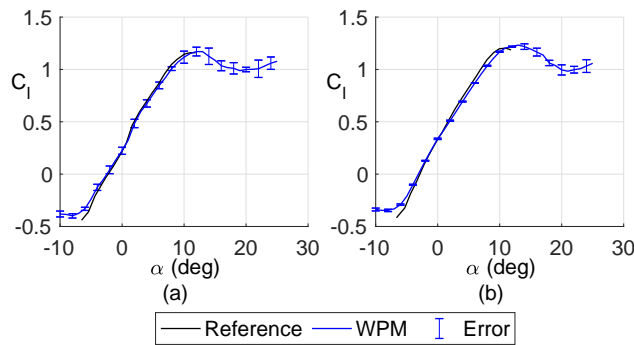


Figure 11. Comparison study of LCM results vs WPM results for SA 7024 airfoil at (a) $Re = 100,000$ and (b) $Re = 300,000$ ²⁵.

$Re = 100,000$ as compared to $Re = 300,000$ and could be attributed to higher model vibrations at lower flow velocities once the airfoil has stalled. Overall, the WPM results match with reference data. Results for the current case study also show that, even though the airfoil is only 6% thick, the flow perturbations are being accurately sensed and captured at the wind tunnel walls.

4.2.4 E387 ($t/c = 9\%$) The Eppler 387 airfoil, commonly used in remote controlled aircraft and ultra-light powered aircraft^{32,33}, was tested with and without a tripwire at Reynolds numbers of 200,000 and 500,000 and compared with LCM data from Selig and McGranahan²⁶. For the tripwire cases, trips sized at 0.11% of the chord in thickness were placed at a 2% chord length distance from the leading edge on the upper surface and 5% chord length distance from the leading edge on the lower surface.

Figure 12(a) shows the WPM results at $Re = 200,000$ accurately predicting the trends in C_l for the E387 airfoil with and without tripped flow. For all positive angles of

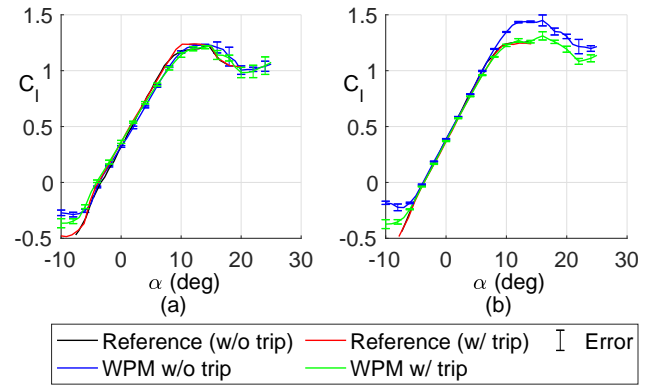


Figure 12. Comparison study of LCM results vs WPM results for Eppler 387 airfoil with and without tripwire at (a) $Re = 200,000$ and (b) $Re = 500,000$ ²⁶.

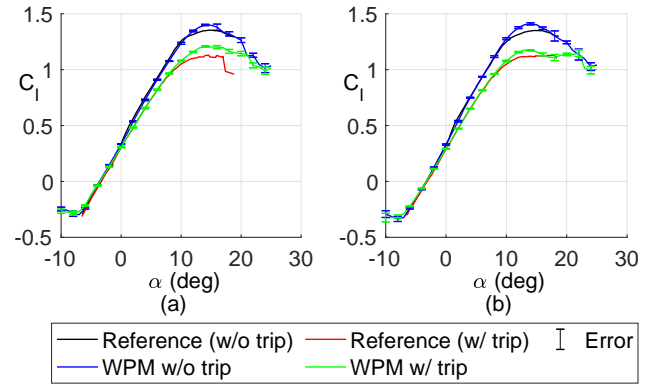


Figure 13. Comparison study of LCM results vs WPM results for Clark Y airfoil with and without tripwire at (a) $Re = 300,000$ and (b) $Re = 400,000$ ²⁷.

attack, while predictions for the clean flow case match very well with expected results, tripped flow results underpredict the lift for $9 \leq \alpha \leq 14$. C_l is also slightly underpredicted at the negative angles of attack for both surface flow conditions.

The WPM method doesn't perform so well for the clean airfoil case at $Re = 500,000$ (Fig. 12(b)), with C_l being overpredicted by $\sim 14\%$ for $\alpha \geq 10$ degrees. Prediction performance of the WPM method for tripped flow conditions improve for positive angles of attack. However, independent of surface flow condition, the WPM underpredicts C_l for $\alpha \leq -6$ degrees. This case shows that the WPM method is very sensitive to the surface flow conditions and is capable of accurately predicting the trends in C_l behavior at said conditions.

4.2.5 Clark Y ($t/c = 12\%$) Clark Y is a flat-bottomed, 12% thick airfoil for low-Reynolds number applications and is very commonly used for model aircrafts. The Clark Y tests were conducted at freestream Reynolds numbers of 300,000 and 400,000, with and without a tripwire. For the tripwire cases, trips sized at 0.19% of the chord in thickness were placed at a 2% chord length distance from the leading edge on the upper surface and 5% chord length distance from the leading edge on the lower surface. WPM C_l predictions compared with LCM results from Selig²⁷ are plotted in Fig. 13.

Overall, the WPM method accurately captures the C_l behavior for the Clark Y airfoil, both qualitatively and

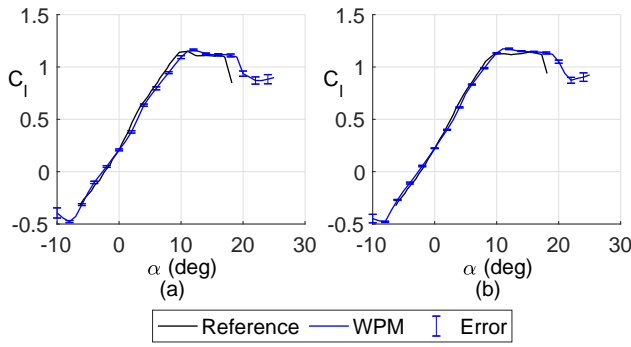


Figure 14. Comparison study of LCM results vs WPM results for Gemini airfoil at (a) $Re = 200,000$ and (b) $Re = 300,000$ ²⁸.

quantitatively, at all tested operating conditions, with a slight deviation in the maximum lift coefficient and stall characteristics for the tripwire case at a Reynolds number of 300,000. Once again, the WPM method was successful in demonstrating its sensitivity by correctly predicting the C_l behavior when the surface flow was tripped.

4.2.6 Gemini ($t/c = 15\%$) The Gemini is a 15% thick airfoil used in sailplanes applications and was tested at Reynolds numbers of 200,000 and 300,000. LCM data for the tests was referenced from Selig et al.²⁸.

Figure 14 shows that the WPM results are in good agreement with the expected results at both freestream Reynolds number conditions. A small deviation in the lift curve slope at $Re = 200,000$, which leads to the stall angle being predicted at 11 degrees instead of 10 degrees, is observed in Fig. 14(a). On the other hand, for the $Re = 300,000$ case (Fig. 14(b)), the lift-curve slope, stall-angle and the maximum lift coefficient are predicted accurately. At both freestream operating conditions, the sharp drop in C_l post-stall is overpredicted by 3 degrees. Overall predictions are well within the expected error range, and hence considered acceptable.

4.2.7 NACA 0018 ($t/c = 18\%$) The symmetric, 18% thick NACA 0018 airfoil was tested at Reynolds numbers of 250,000 and 500,000 and validated against results from Boutillier et. al²⁹ and Timmer et. al³⁰, respectively. WPM results at $Re = 250,000$ (Fig. 15(a)) compare well with reference data at all pre-stall angles of attack but overpredicts α_{stall} by 1 degree and C_l by $\sim 7\%$ for $\alpha < -6$ degrees. Post stall, the WPM predicts the C_l to be $\sim 2.5\%$ above the expected results. WPM lift measurements at $Re = 500,000$ (Fig. 15(b)) show excellent comparison at attached flow conditions but starts to deviate as trailing-edge boundary-layer separation increases ($\alpha \geq 11$ degrees). While $C_{l,max}$ is overpredicted by 4%, stall angle is accurately captured. Post-stall C_l trend varies with sharp drops at 18 and 22 degrees. Altogether, the WPM adequately captures the C_l behavior with small discrepancies in the post-stall regime.

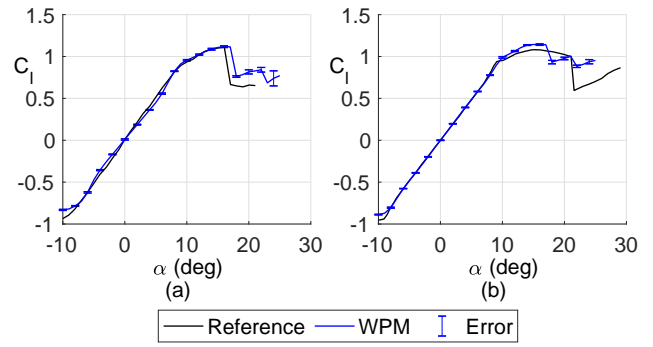


Figure 15. Comparison study of LCM results vs WPM results for NACA 0018 airfoil at (a) $Re = 250,000$ ²⁹ and (b) $Re = 500,000$ ³⁰.

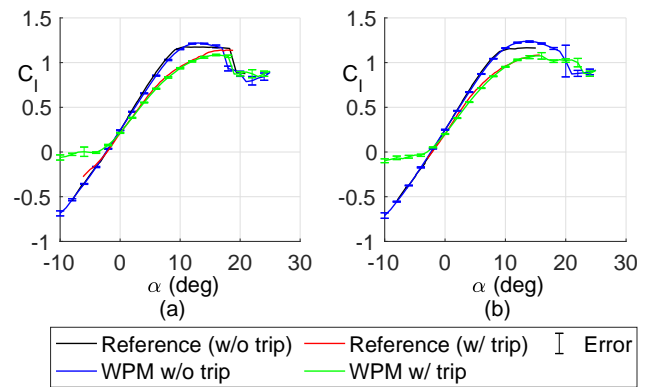


Figure 16. Comparison study of LCM results vs WPM results for S823 airfoil with and without tripwire at (a) $Re = 300,000$ and (b) $Re = 400,000$ ^{28,31}.

4.2.8 S823 ($t/c = 21\%$) The S823 is a 21% thick airfoil used for wind-turbine blades. For the S823, tests were conducted with and without a tripwire for Reynolds numbers of 300,000 and 400,000, and were compared with reference data from Selig et al.^{28,31}. Trips, sized at 0.19% of the chord in thickness, were placed at 2% chord length distance from the leading edge on the upper surface and 10% chord length distance from the leading edge on the lower surface.

From Fig. 16, it can be observed that the WPM method results compare well with the expected results at all angles of attack even after stall for the cases without tripwire. With tripped flow, the results agree well for all positive angles of attack but deviate for negative angles of attack, with WPM results showing earlier flow separation ($\alpha \leq -1$ degree) and overpredicting C_l by $\sim 15\%$. Post-stall C_l at the negative angles of attack for the tripped flow case stays almost constant. Overall, the WPM results comparing well with reference data shows the effectiveness of the method in testing very thick airfoil sections.

5 Conclusion

This research paper discussed the implementation of the Wall Pressure Measurement (WPM) technique to calculate lift as a feasible and quick method to experimentally measure airfoil lift behavior. Though the WPM technique has been implemented in other wind tunnels, little literature exists with regard to the sensitivity of the method to variation in airfoil chord length and thickness. Initial efforts were

focused on conducting a chord sensitivity study to get the optimum airfoil chord to wind tunnel test section length ratio for effective performance of the WPM method. This was followed by a detailed validation study at freestream Reynolds number conditions ranging from 100,000 to 550,000, to test the effectiveness of the WPM test bench in predicting lift data for various airfoil geometries with varying maximum thicknesses and camber.

Results from the chord sensitivity study showed that the WPM method is highly sensitive to the chord of the airfoil and the best results were obtained in the NCSU wind tunnel when the airfoil chord was above 20% of the test section length. However, the 20% scaling ratio did not agree with other implementations of the WPM method and indicated that merely the airfoil chord and test section length were not enough to effectively represent the sensitivity of the WPM method to test section and model geometry. A new design parameter called *CSP* was formulated, taking into account the width of the test section, and was successful in setting a lower limit on the ideal chord-length of the airfoil that would produce the best WPM results for any test-section dimensions. Based on current work and literature, the lower limit of *CSP* was found to be 0.025 which provides a good starting point to model the WPM setup for optimum performance.

Validation study results showed that the C_l predicted by the WPM method is comparable to those measured using the SPM and LCM methods for airfoil geometries with thicknesses ranging from 6% to 21%, with the added advantage of testing with a cheaper and simpler setup that can capture all aerodynamic features without introducing any surface roughness, flow intrusions and arduous calibration procedures. WPM results showed good comparison for cases with tripped flow, implying that even minute flow perturbations were accurately being captured by the method. In a few cases, an increase in Reynolds number resulted in smaller deviations in the results from expected values. In conclusion, the WPM method can serve as a viable, non-intrusive, and inexpensive replacement to existing lift measurement techniques.

Future iterations of this research work will focus on setting an upper limit to the *CSP* with possible extensions focusing on backing the airfoil surface C_p from the wall pressures using theoretical panel methods and machine learning approaches. Implementing the WPM technique for unsteady lift measurements and obtaining the effective shape of the airfoil in unsteady flows can also be explored.

6 Acknowledgment

The authors wish to thank Jim Dean from the College of Design, NC State University, for manufacturing all the required setup, Shaphan Jernigan from the MAE Dept., NC State University, for 3D printing the required airfoils, Samuel Richardson for helping with manufacturing, and the Experimental Aerodynamics team for helping with wind tunnel testing.

References

1. Dudley MR. Experimental techniques for three-axes load cells used at the national full-scale aerodynamics complex. NASA TM 86693, National Aeronautics and Space Administration, 1985.
2. González MA, Ezquerro JM, Lapuerta V et al. Components of a wind tunnel balance: Design and calibration. *Wind Tunnels and Experimental Fluid Dynamics Research* 2011; (1): 115–134.
3. Cole GM and Mueller TJ. Experimental measurements of the laminar separation bubble on an Eppler 387 airfoil at low Reynolds numbers. NASA CR 186263, National Aeronautics and Space Administration, 1990.
4. Althaus D. Measurement of lift and drag in the laminar wind tunnel. Technical report, 2003.
5. Abbott IH, Von Doenhoff AE and Stivers Jr LS. Summary of airfoil data, NACA Rep, 1945.
6. Wolken-Möhlmann G, Knebel P, Barth S et al. Dynamic lift measurements on a FX79W151A airfoil via pressure distribution on the wind tunnel walls. In *Journal of Physics: Conference Series*, volume 75. IOP Publishing, p. 012026.
7. Schneemann J, Knebel P, Milan P et al. Lift measurements in unsteady flow conditions. In *Proceedings of EWECE*.
8. Luhur MR, Peinke J, Schneemann J et al. Stochastic modeling of lift and drag dynamics under turbulent wind inflow conditions. *Wind Energy* 2015; 18(2): 317–337.
9. Ross I and Altman A. Wind tunnel blockage corrections: Review and application to savonius vertical-axis wind turbines. *Journal of Wind Engineering and Industrial Aerodynamics* 2011; 99(5): 523–538.
10. Garner HC, Rogers E, Acum W et al. Subsonic wind tunnel wall corrections. Technical report, Advisory Group For Aerospace Research For And Development Neuilly-Sur-Seine (France), 1966.
11. Mokry M. Subsonic wall interference corrections for half-model tests using sparse wall pressure data. Technical report, National Research Council Canada, 1985.
12. Mokry M. Subsonic wall interference corrections for finite length test sections using boundary pressure measurements. Technical report, Wall Interference in Wind Tunnel, AGARD-CP-335, 1982.
13. Ashill P and Keating R. Calculation of tunnel wall interference from wall-pressure measurements. *The Aeronautical Journal* 1988; 92(911): 36–53.
14. Hackett J, Wilsden D and Lilley D. Estimation of tunnel blockage from wall pressure signatures: a review and data correlation. NASA CR 152241, National Aeronautics and Space Administration, 1979.
15. Hensel RW. *Rectangular-wind-tunnel blocking corrections using the velocity-ratio method*. 2372, National Advisory Committee for Aeronautics, 1951.
16. Allmaras SR. On blockage corrections for two-dimensional wind tunnel tests using the wall-pressure signature method. NASA TR 86759, National Aeronautics and Space Administration, 1986.
17. Johnston J and Gopalarathnam A. Investigation of a bio-inspired lift-enhancing effector on a 2D airfoil. *Bioinspiration & biomimetics* 2012; 7(3): 036003.
18. Havelock TH. The lift and moment on a flat plate in a stream of finite width. *Proceedings of the Royal Society of London*

- Series A Mathematical and Physical Sciences* 1938; 166(925): 178–196.
19. Jacobs EN and Sherman A. Airfoil section characteristics as affected by variations of the Reynolds number. NASA TR 586, National Aeronautics and Space Administration, 1937.
 20. Critzos CC, Heyson HH and Boswinkle Jr RW. Aerodynamic characteristics of NACA 0012 airfoil section at angles of attack from 0 deg to 180 deg. Technical report, National Aeronautics and Space Administration Washington DC, 1955.
 21. Poisson-Quinton P and de Sievers A. Etude aerodynamique dun élément de pale dhélicoptère. In *Agard Conference Proceedings*. 22, pp. 4–1.
 22. Sheldahl RE and Klimas PC. Aerodynamic characteristics of seven symmetrical airfoil sections through 180-degree angle of attack for use in aerodynamic analysis of vertical axis wind turbines. Technical report, Sandia National Labs., Albuquerque, NM (USA), 1981.
 23. Michos A, Bergeles G and Athanassiadis N. Aerodynamic characteristics of NACA 0012 airfoil in relation to wind generators. *Wind Engineering* 1983; : 247–262.
 24. Timmer W. Aerodynamic characteristics of wind turbine blade airfoils at high angles-of-attack. In *3rd EWEA Conference-Torque 2010: The Science of making Torque from Wind, Heraklion, Crete, Greece, 28-30 June 2010*. European Wind Energy Association.
 25. Gopalarathnam A, Broughton BA, McGranahan BD et al. Design of low reynolds number airfoils with trips. *Journal of aircraft* 2003; 40(4): 768–775.
 26. Selig MS and McGranahan BD. Wind tunnel aerodynamic tests of six airfoils for use on small wind turbines. *J Sol Energy Eng* 2004; 126(4): 986–1001.
 27. Selig MS. *Summary of low speed airfoil data Vol. 3*. SoarTech Publications, 1997.
 28. Broeren A, Giguere P, Guglielmo J et al. Summary of Low-Speed Airfoil Data, Vol. 1, 1995.
 29. Boutilier MS and Yarusevych S. Parametric study of separation and transition characteristics over an airfoil at low Reynolds numbers. *Experiments in fluids* 2012; 52(6): 1491–1506.
 30. Timmer W. Two-dimensional low-Reynolds number wind tunnel results for airfoil NACA 0018. *Wind engineering* 2008; 32(6): 525–537.
 31. Selig M, Lyon C, Giguere P et al. *Summary of Low-Speed Airfoil Data, Vol. 2*. SoarTech Publications, 1996.
 32. McGhee RJ. *Experimental results for the Eppler 387 airfoil at low Reynolds numbers in the Langley low-turbulence pressure tunnel*, volume 4062. National Aeronautics and Space Administration, Scientific and Technical Information Division, 1988.
 33. Mueller TJ. Low Reynolds number vehicles. Technical report, Advisory Group For Aerospace Research And Development Neuilly-Sur-Seine (France), 1985.
- | | |
|------------------|--|
| α_{stall} | stall angle of attack |
| b | blockage of airfoil, chord/height of test-section (c/w) |
| c | chord of airfoil |
| C_l | coefficient of lift of airfoil |
| $C_{l,max}$ | maximum coefficient of lift of airfoil |
| C_{li} | design coefficient of lift of airfoil |
| C_p | coefficient of pressure |
| CSP | chord sensitivity parameter |
| η_a | Althaus correction factor for angle of attack |
| η_b | Althaus correction factor for constant pressure distribution |
| η | Althaus correction factor |
| η_x | correction factor for a point vortex |
| l | distance from first pressure port to last pressure port |
| m | distance from center of airfoil to left most pressure port |
| n | distance from center of airfoil to right most pressure port |
| ΔP | change in pressure |
| P_{upper} | static pressure of upper surface |
| P_{lower} | static pressure of upper surface |
| P_R | resulting pressure coefficient for tunnel walls |
| q_∞ | freestream dynamic pressure, $\frac{1}{2}\rho V_\infty^2$ |
| Re | chord Reynolds number |
| ρ | air density |
| sr | scaling facratiotor, $\frac{c}{l} * 100$ |
| l | test section length |
| V | freestream velocity |
| w | test section width |

7 APPENDIX

Notation

α angle of attack